Supplementary Materials for

Reconstitution of the Vital Functions of Munc18 and Munc13 in Neurotransmitter Release

Cong Ma*, Lijing Su*, Alpay B. Seven, Yibin Xu and Josep Rizo

correspondence to: E-mail: cong.ma7@gmail.com (C.M.); jose@arnie.swmed.edu (J.R.)

This PDF file includes:

Materials and Methods

Recombinant proteins

Expression in BL21 *E. coli* cells and purification of full-length rat synaptobrevin and its cytoplasmic domain (residues 29-93), full length rat syntaxin-1A and its cytoplasmic domain (2-253), human SNAP-25B full-length (with its four cysteins mutated to serines), the SNARE motifs of human SNAP-25B (SNN, residues 11-82; and SNC, residues 141-203), full-length rat Munc18-1, rat Munc13-1 MUN domain (residues 859-1407,EF,1453-1531), and the rat synaptotagmin-1 C_2AB fragment (residues 140-421) were described previously (*8, 10, 12, 19, 38-42*). Note that the MUN domain contained a partial deletion in a long loop that promotes aggregation [see (*13, 19*)]. Isotopic labeling to obtain ^{2}H-Ile-$^{13}CH_3$-syntaxin-1 was performed using well-established procedures (*43*).

Expression and purification of C1C2BMUN

To generate a vector to express the C1C2BMUN fragment of rat Munc13-1 with the same loop deletion as the MUN domain (residues 529-1407,EF,1453-1531), we cloned a DNA sequence encoding Munc13-1(529-1531) into the pFastBac^{TM}HT B vector (invitrogen), which contains a polyhedron promoter (for hight-level expression of recombinant protein in insect cell) before the start codon and encodes an N-terminal TEV cleavable His_6 tag. The loop deletion was then performed using QickChange (Stratagene). The construct was used to generate a baculovirus using the Bac-to-Bac system (Invitrogen). Insect cells (sf9) were infected with the baculovirus, harvested about 68-72 hours post-infection, and resuspended in lysis buffer (50mM Tris 8.0, 250mM Nacl, 10mM imidazole). Cells were lysed through one freeze and thaw circle. The cell lysate was centrifuged at 18,000 rpm for 45 minutes, and the clear supernatant was incubated with Ni^{2+}-NTA agarose at 4°C for 2 hours. The beads were washed with: i) lysis buffer; ii) lysis buffer containing 1% TX-100'; iii) lysis buffer containing 1M NaCl; and iv) lysis buffer. The protein was eluted with 200mM imidazole and the His_6-tag was removed by incubation with tobacco etch virus (TEV) protease at 4°C overnight. The protein was further purified by ion exchange chromatography and gel filtration, and was concentrated to 9 mg/ml for storage in 10 mM Tris buffer (pH 8.0) containing 10% glycerol and 250mM NaCl.

Expression and purification of NSF and α-SNAP

NSF and α-SNAP were cloned from a pQE9 vector into a pGEX-KG vector. Both proteins were expressed in BL21 *E.Coli* cells in Luria-Bertani media (LB) media. NSF was induced with 0.4mM IPTG at 20°C for 20h. α-SNAP was induced with 0.4mM IPTG at 25°C for 18h. Cells were re-suspended in a buffer containing 50mM HEPES pH7.6, 400mM KCl, 10% glycerol (v/v), and 2mM dithiothreitol (DTT). The cells were lysed with an Avestin cell disruptor and the lysate was clarified by centrifugation at 20,000 rpm for 30min. The supernatant was incubated with Glutathione Sepharose 4B (GE Healthcare) at 4°C overnight. The bound proteins were washed with phosphate buffered solution (PBS), PBS with 1% TX-100, and then PBS with 500mM NaCl. The GST-tag was cleaved from the proteins by thrombin cleavage at 4°C overnight on the beads. The proteins were further purified by size-exclusion chromatography using a Superdex 75 (for α-SNAP) or Superdex 200 (for NSF) column in a buffer containing 20mM HEPES

pH7.6, 150mM KCl, 10% glycerol (v/v), 1mM DTT. For NSF purification, all buffers contain 0.5mM ATP.

Co-expression and purification of Munc18-1 and full-length syntaxin-1

A pET-DUET vector (Novagen) to co-express N-terminally His_6-tagged full-length rat Munc18-1 and full-length rat syntaxin-1A in BL21 *E. coli* cells was constructed using standard recombinant DNA methods. Cells were grown in LB media and induced with 0.4mM IPTG at an optical density A_{600}=1.0 for 18 h at 23 °C. Cells were harvested and lysed with an Avestin cell disruptor in buffer containing 50mM Tris pH 8.0, 300mM KCl, 10% glycerol, 1% TX-100 and 0.3mM tris(2-carboxyethyl)phosphine (TCEP). The cell lysate was centrifuged at 20,000 rpm for 30 min. The supernatant was incubated with Ni^{2+} - nitrilotriacetic acid (NTA) Agarose (QIAGEN) at room temperature for 1h. The bound proteins were first washed with buffer containing 50mM Tris pH 8.0, 300mM KCl, 10% glycerol (v/v), 0.5% TX-100 and 0.3mM TCEP, and then washed with the same buffer containing 20mM imidazole and 1% 3-[(3-cholamodipropyl)dimethylammonio]-1-propanesulfonate (CHAPS) instead of 0.5% TX-100. The bound proteins were eluted in the same buffer containing 250mM imidazole and 1% CHAPS. The eluted proteins were purified by size-exclusion chromatography using a superdex 200 10/300 column in a buffer containing 20mM Tris pH8.0, 150mM KCl, 10% glycerol (v/v), 1% CHAPS, and 0.5mM TCEP.

We note that octyl-β-D-glucopyranoside (β-OG), a common detergent used in reconstitutions, could not be employed to reconstitute the syntaxin-1-Munc18-1 complex because this detergent dissociates the complex as judged by gel filtration. This finding likely reflects a sensitivity of Munc18-1 to various hydrophobic compounds that were shown to favor dissociation of the Munc18-1-syntaxin-1 complex (*44*). However, use of CHAPS as detergent allowed us to co-purify syntaxin-1 and Munc18-1 by gel filtration (Fig. S3A), and to incorporate this complex in proteoliposomes.

Co-expression and purification of full-length syntaxin-1 and SNAP-25

Recombinant rat full-length syntaxin-1A and human SNAP-25B were co-expressed and purified basically as described (*39*) but with some modifications. BL21 *E. Coli* cells were grown in Terrific Broth media. Cells were induced with 0.4mM IPTG to an optical density A_{600}=1.0 for 20 h at 25°C. Cells were lysed with an Avestin cell disruptor in buffer A (50mM Tris pH8.0, 500mM NaCl, 5% glycerol, 1% TX-100, 20mM imidazole, and 10mM 2-Mercaptoethanol). Cell lysate was clarified by centrifugation at 20,000rpm for 30min. The supernatant was incubated with Ni^{2+}-NTA Agarose (QIAGEN) at room temperature for 1h. The bound proteins were first washed with buffer A, then washed with buffer B (50mM Tris pH8.0, 200mM NaCl, 1% w/v β-OG, 5% glycerol (v/v), and 50mM imidazole), and then eluted with buffer B containing 250mM imidazole instead of 50mM imidazole. The eluted proteins were further purified by ion exchange chromatography on Mono Q with buffers containing 1% β-OG.

NMR spectroscopy

^{1}H-^{13}C HMQC spectra were acquired at 25 ^{o}C on a Varian INOVA800 spectrometer. Samples contained 12-20 μM ^{2}H-Ile-$^{13}CH_3$-syntaxin-1 alone or with different additions (Munc18-1 and/or SNAP-25 were added in a 20% excess). Samples were dissolved in 20

mM Tris (pH 8.0), 150 mM NaCl, 2 mM TCEP, using D_2O as the solvent. Spectra were acquired with a 2.3 hour total acquisition time.

Fluorescence resonance energy transfer (FRET) assays to monitor t-SNARE disassembly and SNARE complex assembly experiments

Purified synaptobrevin SNARE motif (residues 29-93) with a S61C mutation and SNAP-25 SNC (residues 141-203) with a S187C mutation were labeled in PBS buffer (20 mM sodium phosphate, pH 7.4, 100 mM NaCl) by adding a 20× molar excess of BODIPY-FL maleimide (Invitrogen). Purified syntaxin-1(2–253) containing C145S, S249C mutations was labeled using a 20× molar excess of tetramethylrhodamine-5-iodoacetamide dihydroiodide (5-TMRIA) (Invitrogen). After incubation at 4 °C overnight, the reactions were stopped by adding 10 mM DTT. Free dyes were removed by ion-exchange (source Q) chromatography followed by gel filtration on a Superdex 200 column. Labeled proteins were dialyzed against buffer C (25 mM HEPES, pH 7.4, 150 mM KCl, 1mM DTT, 10% glycerol (v/v)) at 4 °C overnight. Complex assembly or disassembly experiments were carried out on a Photon Technology Incorporated Spectrofluorometer (PTI). All experiments were conducted at 30°C in buffer C. BODIPY-FL labeled proteins were excited at 485 nm, and the emission intensity was monitored at 513 nm. In experiments to monitor displacement of SNAP-25 from syntaxin-1 by Munc18-1, t-SNARE complexes between SNN, SNC(S187C)-BODIPY and syntaxin-1(2-253)(C145S, S249C)-5-TMRIA were pre-assembled overnight and Munc18-1 was then added. Release of SNC was monitored through the resulting increase in the BODIPY-FL fluorescence due to loss of FRET with the 5-TMRIA acceptor. The fluorescence was normalized to the maximum value predicted by extrapolation after fitting the data to an exponential rise, and setting the initial fluorescence to 0. SNARE complex assembly experiments monitored by FRET were performed using synaptobrevin(29-93)(S61C)-BODIPY-FL and syntaxin-1(2-253)(C145S, S249C)-5-TMRIA as described previously (*13*). FRET efficiency was calculated according to $E = (F_0–F_{obs})/F_0$, where F_0 is the fluorescence intensity at time 0 and F_{obs} is the fluorescence intensity measured as a function of time.

Liposome co-floatation assays

Proteoliposomes containing syntaxin-1-Munc18-1 complex were prepared as described below with a protein/lipid (P/L) ratio of 1:1000. Solutions containing 4 mM lipids (4 μM syntaxin-1-Munc18-1 complex) were incubated with 10 μM SNAP-25 at room temperature for 1 hr. The proteoliposomes and bound proteins were isolated by floatation on a Histodenz density gradient (40%:35%:30%) as described (*39*). Samples from the top of the gradient (35 μl) were taken and analyzed by SDS-PAGE and Coomassie blue staining. For experiments with reconstituted full-length syntaxin-1, proteoliposomes containing PC:PE:PS:PIP2 (60:18:20:2) at a P/L ratio of 1:500 were prepared as previously described for a syntaxin-1(183-288) fragment (*40*). The syntaxin-1 proteoliposomes were then dialyzed with 1g/L Bio-beads SM2 (Bio-Rad) 3 times in 25mM HEPES pH7.3, 150mM KCl, 10% glycerol (v/v) at 4°C overnight to remove the detergent. The syntaxin-1 liposomes were incubated with SNAP-25 at 4°C for 2h and contained 3 μM syntaxin-1 and 6 μM SNAP-25 after addition of different reagents, which included 5 μM Munc18-1, 0.5μM NSF, 1 μM α-SNAP, 2 mM ATP, 5 mM $MgCl_2$ or 5 mM EDTA. After incubation at 37°C for 1 hr, the proteoliposomes were isolated by

floatation on a Histodenz density gradient (40%:35%:30%) and samples at the top (35 μl) were taken and analyzed by SDS-PAGE and Coomassie blue staining.

Lipid mixing assay using syntaxin-1-Munc18-1 liposomes

All lipids were purchased from Avanti Polar Lipid. Donor (synaptobrevin) liposomes contained 60% POPC, 17% POPE, 20% DOPS, 1.5% NBD-PE and 1.5% Rhodamine-PE. Acceptor (syntaxin-1-Munc18-1) liposomes contained 58% POPC, 20% POPE, 18% DOPS, 2% PIP2 and 2% DAG. Lipid mixtures were dried in glass tubes with nitrogen gas and under vacuum overnight. Lipid films were re-suspended in buffer buffer C (25 mM HEPES, pH 7.4, 150 mM KCl, 1mM DTT, 10% glycerol (v/v)) and vortexed for at least 5 min. The re-suspended lipid films were frozen and thawed five times, and then extruded through a 50 nm polycarbonate filter with an Avanti extruder for at least 29 times. Purified proteins in buffer containing 1% CHAPS were added slowly to liposomes (5 mM lipids) to make the final concentration of CHAPS 0.4%. The P/L ratio ranged from 1:500 to 1:1000 for the synaptobrevin liposomes, and from 1:1000 to 1:2000 for the syntaxin-1-Munc18-1 liposomes. The liposome protein mixtures were incubated at room temperature for 40 min and then dialyzed extensively with 1g/L Bio-beads SM2 (Bio-Rad) 3 times in 20mM Hepes, pH 7.4, 150mM KCl, 1mM DTT, 10% glycerol (v/v) at 4 °C. For lipid mixing assays, donor liposomes (0.25 mM lipids) were mixed with acceptor liposomes (0.5 mM lipids) in the presence of 1 μM C1C2BMUN, 5 μM SNAP-25, 2 μM C_2AB fragment and/or 0.5 mM Ca^{2+} (as indicated in the figures) in a total volume of 80 μl. NBD fluorescence emission at 538 nm (excitation 460 nm) was monitored with a PTI Spectrofluorometer. All experiments were performed at 30 °C. At the end of each reaction, 1% w/v β-OG was added to solubilize the liposomes. We routinely checked that the observed increases in NBD fluorescence intensity reflected true dequenching rather than light scattering caused by liposome clustering [see (*45*)].

Because of considerable variability in the fluorescence intensity observed upon detergent addition, which may arise from partial precipitation, we find that we obtain more consistent results by first converting the time traces to *F1/F0*, where *F1* is the observed fluorescence intensity and *F0* is the initial intensity, and then we average the *F1/F0* value observed upon detergent addition for an entire set of experiments. This average is then used to normalize all the traces to express the data as % of maximum fluorescence.

All comparisons of lipid mixing efficiencies induced by diverse reagents shown in the figures were performed in sets of experiments with the same proteoliposome preparations. In each set, we repeated at least three times the experiments that were most crucial for the conclusions of this work, while some of the controls were repeated only two times because of the limited lifetime of the preparations. The lipid mixing efficiencies observed under the same conditions, expressed as % of maximum florescence at 1,000 s, were averaged and the standard deviations calculated. There is a natural variability in the efficiency of lipid mixing observed in these reconstitution assays with different proteoliposome preparations in terms of absolute values, but the relative efficiencies resulting from different additions were reproducible in separate sets of experiments.

Lipid mixing assay using syntaxin-1-SNAP-25 liposomes

Donor (synaptobrevin) liposomes and acceptor (syntaxin-1-SNAP-25) liposomes contained the same lipid compositions described above. Lipid mixtures were dried in glass tubes with nitrogen gas and under vacuum overnight. Lipid films were re-suspended and dissolved in buffer C with 1.2% β-OG. Purified proteins in buffer containing 1% β-OG were added to liposomes (5 mM lipids) to make the P/L ratio 1:600. The mixtures were incubated at room temperature for 40 min and dialyzed extensively with 1g/L Bio-beads SM2 (Bio-Rad) 3 times in buffer C. For lipid mixing assays, donor liposomes (0.25 mM) were mixed with acceptor liposomes (0.5 mM) with different additions in a total volume of 80 µl. For experiments with NSF-α-SNAP, acceptor liposomes were first incubated with 0.1 µM NSF, 0.5 µM α-SNAP, 5 mM $MgCl_2$ and 2 mM ATP at 37°C for 20min, and then mixed with donor liposomes with different additions, which included 0.5 µM Munc18-1, 1 µM C1C2BMUN, 2 µM C_2AB fragment, 0.5 mM Ca^{2+}, and excess SNAP-25 as indicated in the figures. All experiments were performed at 37°C. At the end of each reaction, 1% w/v β-OG was added to solubilize the liposomes, and the data were analyzed as described above for the lipid mixing assays with syntaxin-1-Munc18-1 liposomes.

Leakiness assay

Content mixing assays have commonly been hindered by the tendency of small molecules to leak from SNARE-containing proteoliposomes [e.g. see (*46-48*)]. However, synaptobrevin-liposomes with encapsulated sulforhodamine were recently reported to have very slow leakage rates that allowed monitoring of content mixing from dequenching of sulforhodamine upon fusion with acceptor liposomes (*26*). To test for donor liposome leakiness, we prepared synaptobrevin liposomes containing sulforhodamines and monitored its fluorescence emission intensity at 587nm (excited at 565nm). In our hands, a small amount of leakiness of sulforhodamine trapped into synaptobrevin-liposomes was observed when standard methods were used to prepare the proteoliposomes, and addition of C1C2BMUN exacerbated the leakiness (Fig. S5A), likely because of sensitivity to residual detergent. However, we were able to minimize this problem through extensive dialysis of the liposomes against buffer with detergent-absorbing beads in small volumes, as described next, resulting in a very slow degree of leakiness that can be readily subtracted from signal increases due to content mixing (Fig. S5B).

Content mixing assay

Donor (synaptobrevin) liposomes contained 44.5% POPC, 20% POPE, 12% DOPS, 20% cholesterol, 3.5% DiD (Invitrogen). Lipid mixtures were dried in glass tubes with nitrogen gas and under vacuum overnight. Lipid films were re-suspended and dissolved in buffer C containing 1% w/v β-OG and 40mM sulforhodamine B (Acros Organics). Purified full-length synaptobrevin in buffer containing 1% w/v β-OG was added to the lipid mixtures to make the final concentration of lipids 5mM and the P/L ratio 1:500. The protein lipid mixtures were diluted 4 times (keeping the sulforhodamine concentration at 40mM) to allow liposome formation, and then were incubated at room temperature for 40 min. The liposomes were purified with a Superose 6 column. The first 1 ml sample coming out in the void volume was collected and dialyzed in 150 ml detergent free buffer

(20 mM Hepes, pH 7.4, 150 mM KCl, 1mM DTT) containing 10 g of Amberlite XAD2 3 times at 4 ^{o}C (2 times 2 hr and one time overnight). The resulting lipid concentration was determined by UV. Acceptor (syntaxin-1-Munc18-1) liposomes were prepared with the same method described for the lipid mixing assays. Lipid mixing and content mixing were monitored as described for the lipid mixing assays by measuring de-quenching of DiD (excited at 650nm, emission at 675nm) and sulforhodamine B (excited at 565nm, emission at 587nm). The data were analyzed and quantified as described above for the lipid mixing assays that monitored NBD fluorescence de-quenching.

In these experiments, two clearly distinct outcomes are expected if true content mixing occurs or the content of the donor vesicles is released due to lysis. Thus, since our NBD fluorescence de-quenching assays (Fig. 2) indicate that donor vesicles undergo an average of 1.5 to 2 rounds of fusion based on a standard conversion method (*49*), content release upon vesicle lysis should lead to a monotonous increase in sulforhodamine fluorescence intensity that would saturate close to the maximal signal observed upon detergent addition. In contrast, bona-fide content mixing should result in increases in sulforhodamine fluorescence intensity that saturate at lower intensities and follow a similar time course as lipid mixing, just a we observed in the experiments where we added SNAP-25, C1C2BMUN, C_2AB fragment-Ca^{2+} (Fig. 3).

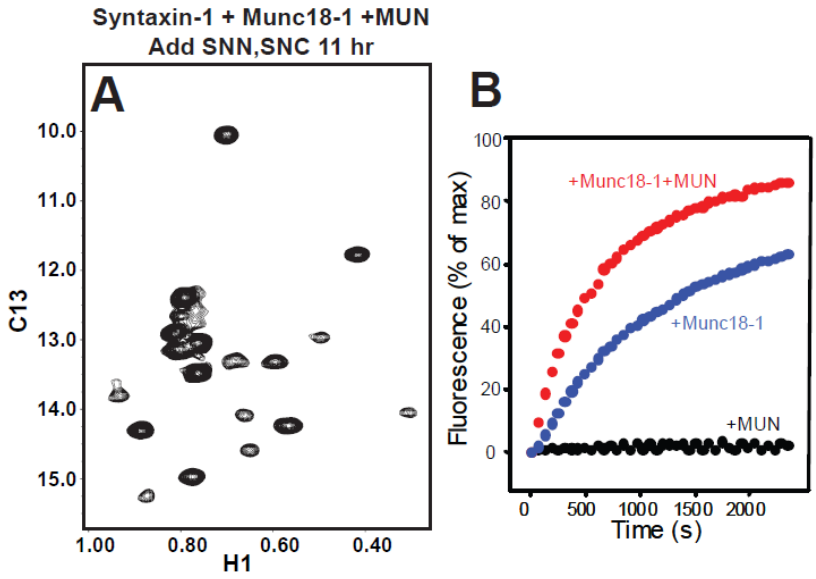

Fig. S1.

Munc18-1 displaces SNAP-25 from syntaxin-1 in solution. (**A**) ^{1}H-^{13}C HMQC spectrum of ^{2}H-Ile-$^{13}CH_3$-syntaxin-1 initially bound to Munc18-1 and then incubated with the SNAP-25 SNARE motifs (SNN and SNC) for 11 hr in the presence of the Munc13-1 MUN domain. (**B**) The Munc13-1 MUN domain accelerates the transition from the syntaxin-1-SNAP-25 complex to the syntaxin-1-Munc18-1 complex. Syntaxin-1 cytoplasmic region (residues 2-253) labeled with rhodamine at residue 249 was incubated with SNN and SNC that was labeled with BODIPY at residue 187. The BODIPY fluorescence, which decreases upon formation of the syntaxin-1-SNN-SNC complex due to efficient FRET with the rhodamine label on syntaxin-1, was monitored and the sample was incubated until the BODIPY fluorescence reached a plateau that indicated completion of the reaction. Munc18-1, Munc13-1 MUN domain or both were added and then we monitored the increase in BODIPY fluorescence resulting from loss of FRET as syntaxin-1 binds to Munc18-1 and SNN-SNC are released. The three curves were normalized to the extrapolated maximum fluorescence in the presence of Munc18-1 and MUN domain.

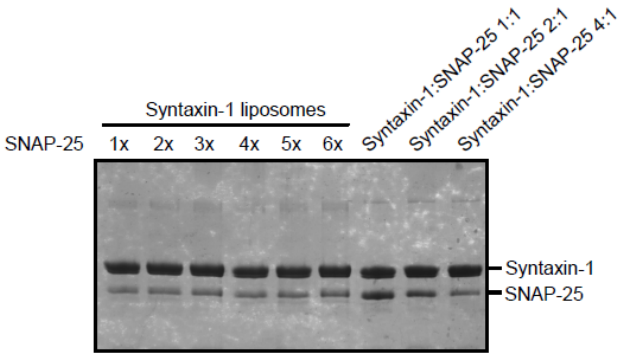

Fig. S2

SNAP-25 binds efficiently to reconstituted syntaxin-1. Syntaxin-1-containing liposomes were incubated with different amounts of SNAP-25 (from 1:1 to 1:6 ratio as indicated) and the samples were analyzed with co-flotation assays followed by SDS-PAGE and Coomassie Blue staining (six lanes on the left). Three control samples containing a constant amount of syntaxin-1 (3.3 μg) and different amounts of SNAP-25 (syntaxin-1 to SNAP-25 ratios of 1:1, 2:1 and 4:1 as indicated) were loaded for comparison purposes (three lanes on the right). The co-floatation assays suggest that a similar amount of SNAP-25 was bound to syntaxin-1 in all samples; this amount corresponds to a syntaxin-1-SNAP-25 ratio of approximately 4:1 based on comparison with the control samples. These observations are consistent with studies that revealed a 2:1 stoichiometry for syntaxin-1-SNAP-25 complexes in solution (*50*), and with the expectation that only about half of the syntaxin-1 molecules are available for binding because the other half is oriented inside the liposomes.

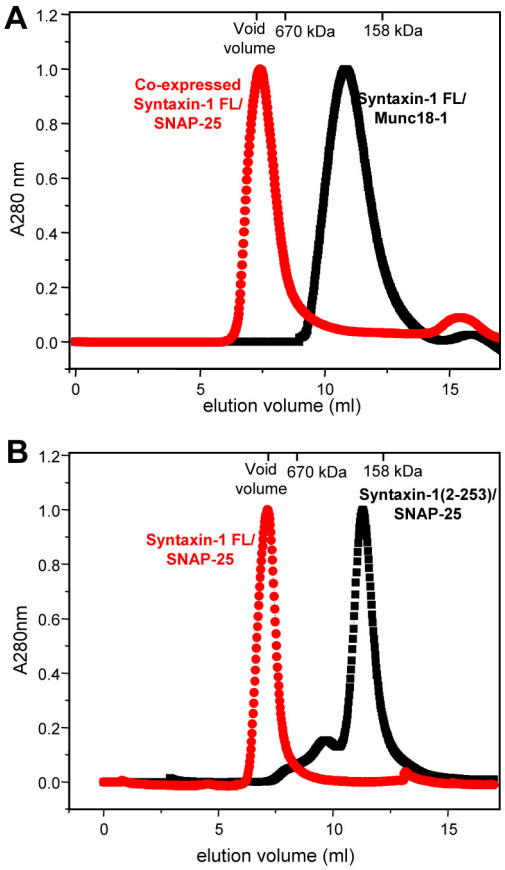

Fig. S3

Syntaxin-1-SNAP-25 complexes readily aggregate. (**A,B**) Gel filtration profiles on Superdex200 of co-expressed full-length (FL) syntaxin-1 and SNAP-25 complex (red) or FL syntaxin-1 and Munc18-1 complex (black) (**A**), and of FL syntaxin-1-SNAP-25 complex (red) or syntaxin-1(2-253)-SNAP-25 complex formed with separately expressed proteins. The void volume and the elution volumes of molecular weight standards are indicated at the top. Note that the buffer used for chromatography contained 1% CHAPS and, as a result of solvation with detergent micelles and the elongated nature of the complexes, monomeric complexes elute considerably earlier than expected from their molecular weights. Nevertheless, the elution of the FL syntaxin-1-SNAP-25 complexes with the void volume clearly shows the formation of aggregates which may arise at least in part from participation of the two SNARE motifs of one SNAP-25 molecule in different four-helix bundles with syntaxin-1 and other SNAP-25 molecules (see Fig. 5). In all chromatograms, the UV absorbance at 280 nm was normalized to the maximum value.

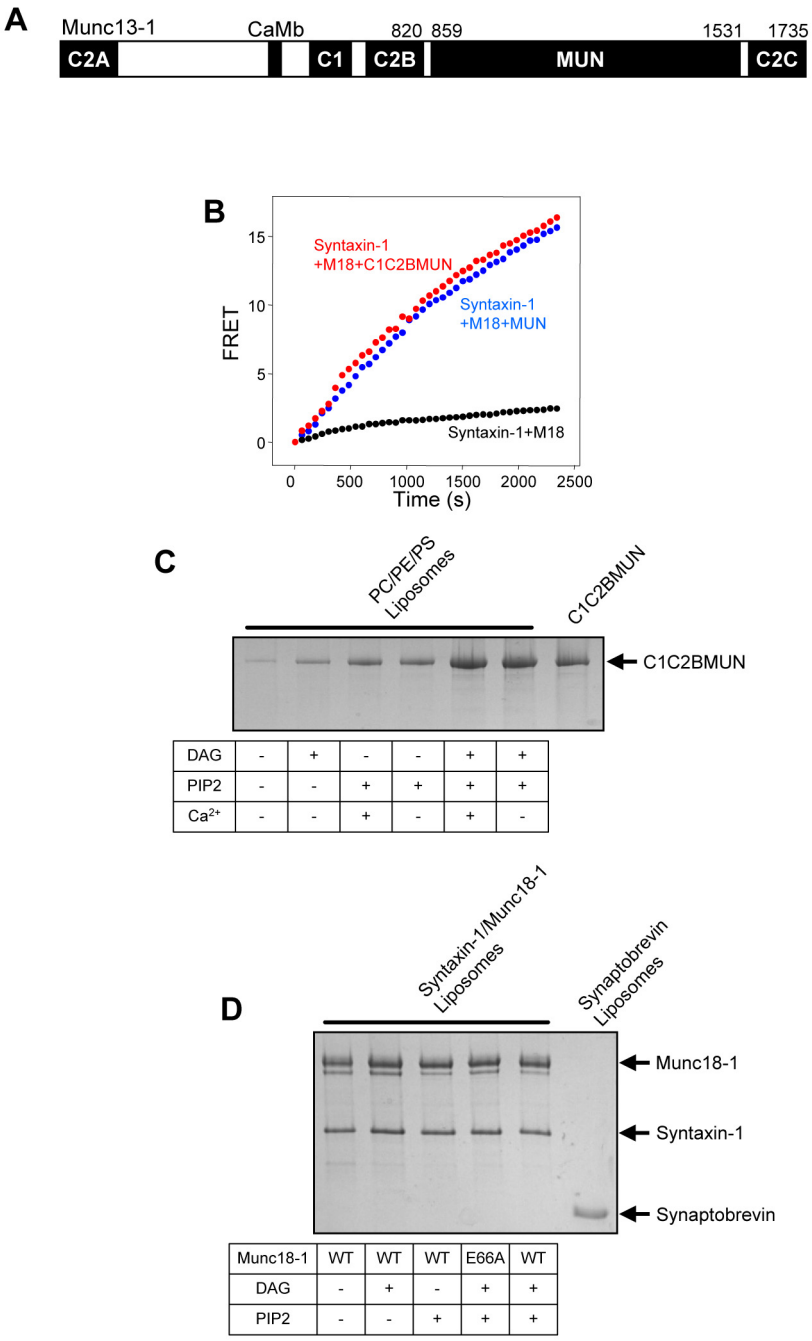

Fig. S4

Characterization of the Munc13-1 C1C2BMUN fragment and reconstituted proteoliposomes. (**A**) Domain diagram of rat Munc13-1. Residue numbers indicate selected domain boundaries. The three C_2 domains, the C_1 domain and the MUN domain are labeled C2A-C2C, C1 and MUN, respectively. CaMb indicates a calmodulin-binding sequence. (**B**) To perform some basic characterization of the Munc13-1 C1C2BMUN fragment, we tested whether it can accelerate the transition from the syntaxin-1-Munc18-

1 complex to the SNARE complex using a FRET assay as described for the Munc13-1 MUN domain (*13*). The diagram shows the time dependence of FRET between a BODIPY fluorescence donor probe placed on residue 61 of the synaptobrevin SNARE motif and a rhodamine acceptor probe placed on residue 249 of syntaxin-1(2-253) as they form the SNARE complex with the SNARE motifs of SNAP-25. Reactions were performed as described (*13*) and started with the labeled syntaxin-1(2-253) bound to Munc18-1 in the absence or presence of MUN domain or C1C2BMUN fragment. Both fragments led to a similar acceleration of SNARE complex formation. (**C**) The C_1 and C_2B domain mediate binding of Munc13-1 to diacylglycerol (DAG) (*30*) and phosphatidylinositol-4,5-bisphosphate (PIP2) (*31*). To test whether the C1C2BMUN fragment can bind to these lipids, we performed co-floatation assays of Munc13-1 C1C2BMUN fragment with liposomes containing PC, PE and PS, and containing or lacking DAG or PIP2 as indicated. Experiments with PIP2 were performed in the presence or absence of Ca^{2+}, revealing some Ca^{2+}-dependent enhancement of binding. (**D**) SDS-PAGE analysis, monitored by Coomassie Blue staining, of the syntaxin-1-Munc18-1-liposomes and the synaptobrevin-liposomes used in the reconstitution experiments of Figs. 2,3. The gel shows that the results shown in Figs. 2G-J do not arise because of substantial differences in the amount of reconstituted syntaxin-1-Munc18-1 complex.

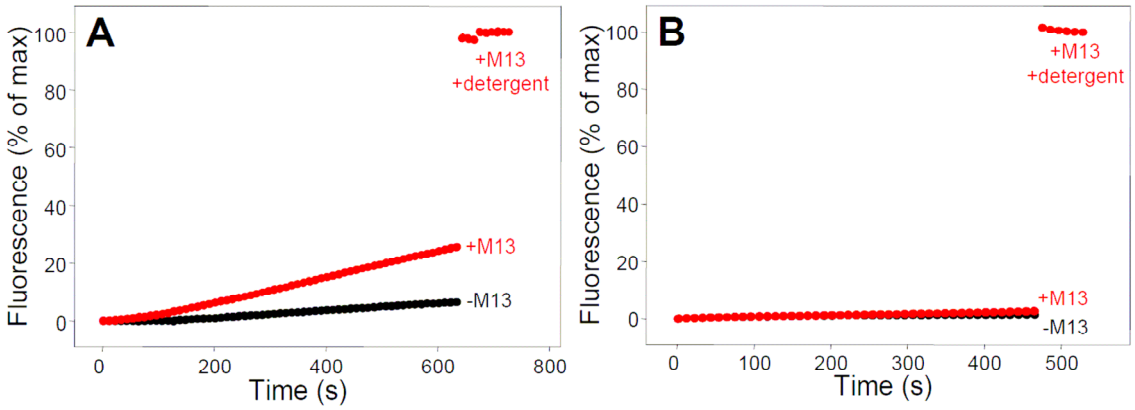

Fig. S5

Analysis of donor liposome leakiness. (**A,B**) The sulforhodamine fluorescence intensity of synaptobrevin-donor liposomes was monitored as a function of time in the absence or presence of Munc13-1 C1C2BMUN fragment. In (**A**), the liposomes were prepared by standard methods as described (*26*). In (**B**), the same procedure was followed except that dialysis was performed against BioBeads (BioRad) in small volumes to remove the detergent more efficiently.

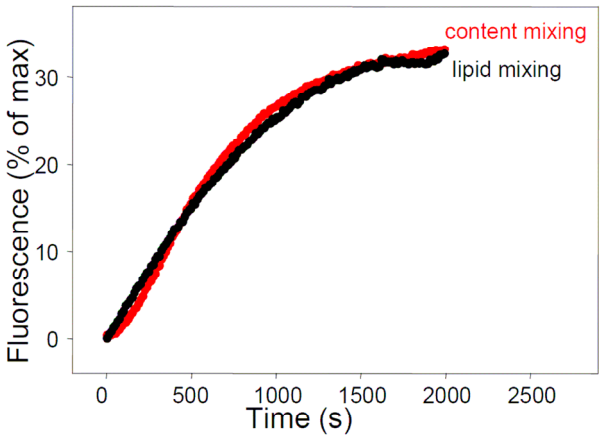

Fig. S6

Content mixing correlates with lipid mixing. The diagram shows a superposition of the content-mixing and lipid-mixing traces observed in the presence of SNAP-25, C1C2BMUN, C_2AB fragment and 0.5 mM Ca^{2+} in the experiments described in Fig. 3.

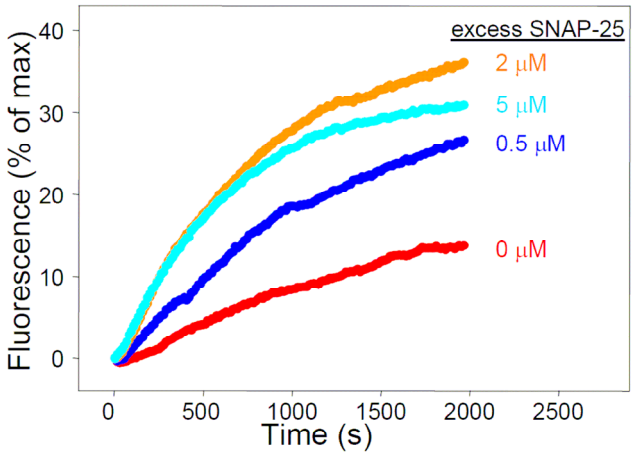

Fig. S7

Dependence of lipid-mixing efficiency on SNAP-25 excess. The diagram shows the lipid mixing observed in experiments performed as in Fig. 4A in the presence of Munc18-1, C1C2BMUN, C_2AB fragment, NSF, α-SNAP, Mg^{2+}-ATP and 0.5 mM Ca^{2+} as function of added SNAP-25 excess.

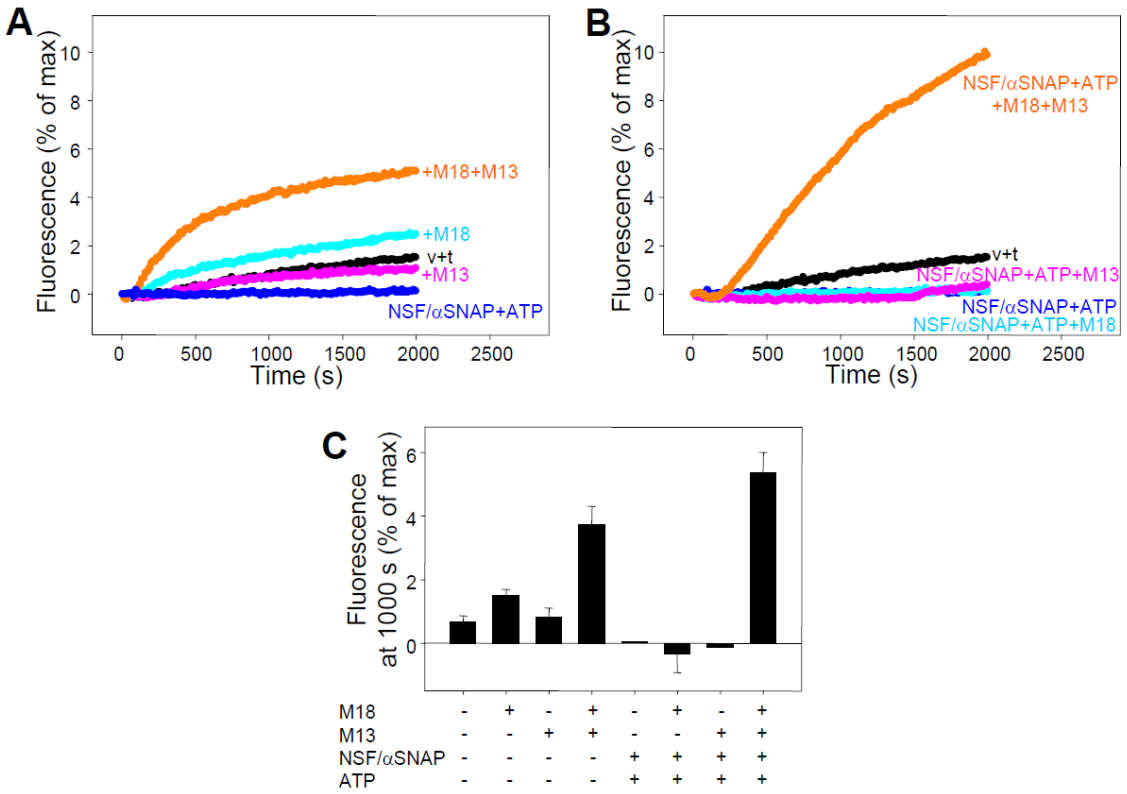

Fig. S8

NSF-α-SNAP inhibit lipid mixing between syntaxin-1-SNAP-25-liposomes and synaptobrevin-liposomes, and Munc18-1-Munc13-1 activate lipid mixing. (**A**,**B**) Traces showing the lipid mixing observed between acceptor liposomes containing syntaxin-1-SNAP-25 heterodimers (separately expressed proteins) and synaptobrevin donor liposomes containing NBD-lipids quenched by rhodamine-lipids in the presence of Munc18-1 (M18), Munc13-1 C1C2BMUN (M13), NSF, α-SNAP and/or Mg^{2+}-ATP in various combinations (v+t indicates the lipid mixing observed with no additions). All samples contained an excess of 2 μM SNAP-25. Samples containing C1C2BMUN also included 0.5 mM Ca^{2+}. The y axis represents NBD fluorescence normalized to the maximum fluorescence observed upon detergent addition. (**C**) Quantification of the results obtained in the experiments of (**A**,**B**). Error bars represent standard deviations. In **A**, the black trace (v+t) shows that lipid mixing between the synaptobrevin-liposomes and the syntaxin-1-SNAP-25 liposomes was inefficient under the conditions of our experiments, that Munc18-1 enhanced lipid mixing moderately, and that Munc18-1 together the Munc13-1 C1C2BMUN fragment stimulated lipid mixing more strongly, revealing a synergy between them. NSF-α-SNAP completely abolished the lipid mixing induced by the SNAREs alone. Panel **B** shows that Munc18-1 alone or the Munc13-1 C1C2BMUN fragment alone could not overcome the inhibition caused by NSF-α-SNAP, but together they dramatically activated lipid mixing. These results show that Munc18-1 and Munc13-1 can also stimulate lipid mixing in an NSF-α-SNAP-resistant manner in the absence of the synaptotagmin-1 C_2AB fragment, although the overall lipid mixing is

less efficient because of the lack of the activity of the Ca^{2+} sensor (note the different scale of the y axis in panels **A-C** compared to those in Fig. 4).

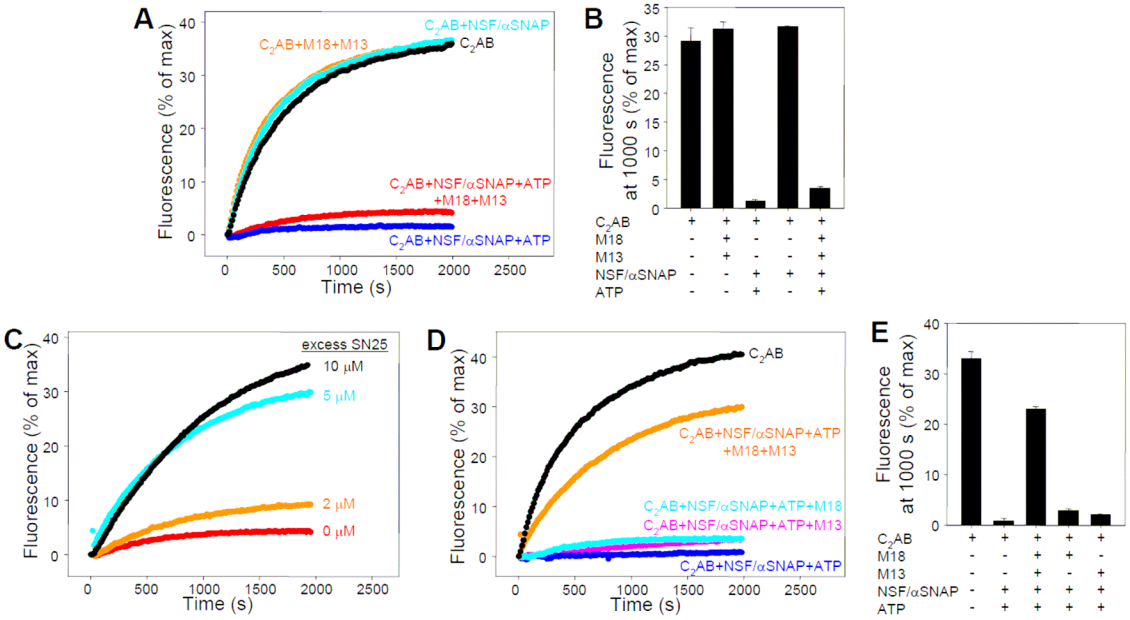

Fig. S9

NSF-α-SNAP inhibit lipid mixing between co-expressed syntaxin-1-SNAP-25-liposomes and synaptobrevin-liposomes, and Munc18-1-Munc13-1 activate lipid mixing. The experiments were performed as in Figure 5, except that the reconstituted syntaxin-1 and SNAP-25 were co-expressed. (A) Traces showing the lipid mixing observed in the presence of Munc18-1 (M18), Munc13-1 C1C2BMUN (M13), synaptotagmin-1 C_2AB fragment (C_2AB), NSF, α-SNAP and/or Mg^{2+}-ATP in various combinations. All experiments were performed in the presence of 0.5 mM Ca^{2+}. The y axis represents NBD fluorescence normalized to the maximum fluorescence observed upon detergent addition. (**B**) Quantification of the results obtained in the experiments of (**A**). (**C**) Lipid mixing observed in the presence of Munc18-1, C1C2BMUN, C_2AB fragment, NSF, α-SNAP, Mg^{2+}-ATP and 0.5 mM Ca^{2+} as function of added SNAP-25 excess. (**D**) Lipid mixing experiments performed as in (**A**) with various additions, all in the presence of 5 μM SNAP-25 excess. (**E**) Quantification of the results of panel (**D**). Error bars represent standard deviations.

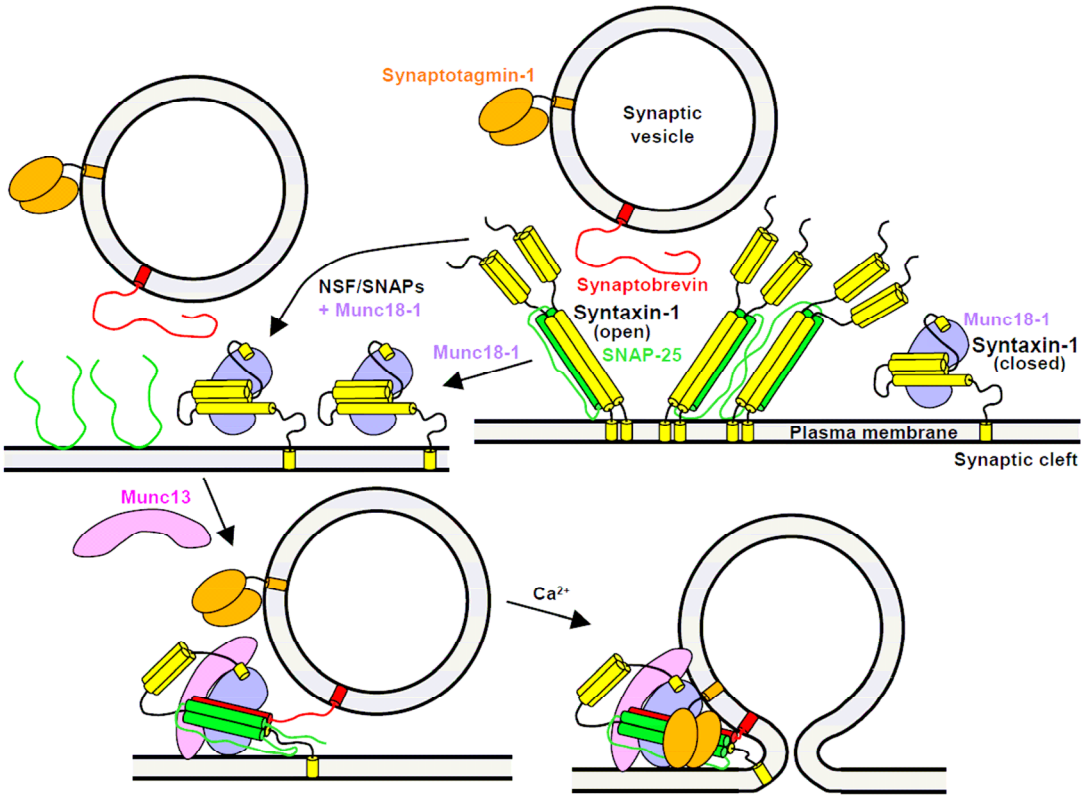

Fig. S10

Model of synaptic vesicle fusion integrating the function of eight major components of the release machinery. A key postulate of this model is that syntaxin-1-SNAP-25 heterodimers are not part of the pathway that leads to fusion, and they are converted to syntaxin-1-Munc18-1 complexes directly by displacement of SNAP-25 with Munc18-1, or indirectly by disassembly of the heterodimers by NSF-α-SNAP followed by capture of the released syntaxin-1 by Munc18-1. It is plausible that the activity of NSF-α-SNAP in disassembling syntaxin-1-SNAP-25 heterodimers is an 'accident' reminiscent of its 'true' function in disassembling the SNARE complex. However, if syntaxin-1-SNAP-25 heterodimers were bona-fide starting points for synaptic vesicle fusion, it seems that the constant formation of these heterodimers and their disassembly by NSF/SNAPs would result in a futile waste of energy. Thus, we favor the view that the activity of NSF/SNAPs on syntaxin-1-SNAP-25 heterodimers serves an important function. In this context, we note that sequences that form long coiled coils such as SNARE motifs are often promiscuous, which is particularly emphasized by the tendency of the syntaxin-1 SNARE motif to bind to many proteins (*51*), to form a tetramer (*52*), and to associate with SNAP-25 in different forms (*53*), including 2:1 complexes where synaptobrevin is replaced by a second syntaxin-1 unit (*54*) (see upper right panel). These findings also reflect a tendency of SNARE motifs to form four-helix bundles rather than three-helix bundles. Thus, while a widespread model depicts a syntaxin-1-SNAP-25 heterodimer as a three-helix bundle formed by the SNARE motif of syntaxin-1 and the two SNARE motifs of SNAP-25, and envisions that this three-helix bundle serves as the acceptor for synaptobrevin to form the

SNARE complex, the three-helix bundle is unstable, hence the tendency of syntaxin-1-SNAP-25 heterodimers to have a 2:1 stoichiometry (*55*). The three-helix bundles can be favored using a large excess of SNAP-25 (*55*), but this mechanism is unlikely to operate in vivo because syntaxin-1 is very abundant in the plasma membrane. Note also that oligomeric t-SNARE complexes can be formed when the two SNARE motifs of one SNAP-25 molecule form separate four-helix bundles (see upper right panel). Hence, syntaxin-1-SNAP-25 heterodimers constitute a heterogeneous mixture of complexes. These observations led us to propose that syntaxin-1-SNAP-25 heterodimers constitute a poor starting point for fusion and that the activity of NSF-α-SNAP in disassembling these heterodimers serves an important function that allows generation of a better-defined starting point for membrane fusion. It is also important to note that Secp18p-Sec17p (the yeast homologues of NSF-α-SNAP) also act on yeast vacuolar t-SNARE complexes (*35*), suggesting that this may be a general function in intracellular membrane traffic.

Our finding that Munc13 and Munc18-1 can orchestrate SNARE complex formation and membrane fusion in an NSF-SNAP-resistant manner establishes an additional similarity with results obtained in studies of yeast vacuolar fusion, where the HOPS tethering complex performs a similar function (*35, 36*). The recent finding of sequence and structural similarity between the Munc13 MUN domain and subunits of tethering factors that function in diverse membrane compartments (e.g. exocyst, GARP, Cog and Dsl1) indicated that Munc13 has a general function that is shared with these factors (*18, 19*). However, these tethering factors form part of large complexes with multiple subunits, and tethering complexes from other membrane compartments that do not exhibit sequence homology with Munc13, such as HOPS and TRAPP, also contain multiple subunits. Hence, it was highly unclear whether Munc13 by itself could play similar roles as these tethering complexes. The parallel nature of our results and those obtained in yeast vacuolar fusion uncovers a clear similarity between very remote membrane fusion systems and suggests that Munc18-1-Munc13 share this fundamental function with all SM proteins and corresponding tethering complexes. At the same time, the diversity in the architecture of tethering complexes suggests that, even if they share a common function in orchestrating SNARE complex assembly, they may accomplish this function by different mechanisms that respond to different regulatory requirements. For instance, the closed conformation of syntaxin-1 is not adopted by the vacuolar syntaxin Vam3p (*56*), and the Munc18-1-syntaxin-1 complex appears to be a specialization of regulated secretion (*8, 57*). Correspondingly, the Munc13 MUN domain has a general role in coordinating SNARE complex assembly and a specific role in opening syntaxin-1. Note also that some of the details of the interplay between HOPS and Sec18p-Sec17p (*35, 36*) differ from the interplay between Munc18-1-Munc13 and NSF-α-SNAP described here, and that vacuolar fusion does not require synaptotagmin-1-Ca^{2+}.

References

1. J. Rizo, C. Rosenmund, Synaptic vesicle fusion. *Nat. Struct. Mol. Biol.* **15**, 665 (2008).
2. T. C. Sudhof, J. E. Rothman, Membrane fusion: grappling with SNARE and SM proteins. *Science* **323**, 474 (2009).
3. T. Sollner, M. K. Bennett, S. W. Whiteheart, R. H. Scheller, J. E. Rothman, A protein assembly-disassembly pathway in vitro that may correspond to sequential steps of synaptic vesicle docking, activation, and fusion. *Cell* **75**, 409 (1993).
4. P. I. Hanson, R. Roth, H. Morisaki, R. Jahn, J. E. Heuser, Structure and conformational changes in NSF and its membrane receptor complexes visualized by quick-freeze/deep-etch electron microscopy. *Cell* **90**, 523 (1997).
5. R. B. Sutton, D. Fasshauer, R. Jahn, A. T. Brunger, Crystal structure of a SNARE complex involved in synaptic exocytosis at 2.4 A resolution. *Nature* **395**, 347 (1998).
6. M. A. Poirier *et al.*, The synaptic SNARE complex is a parallel four-stranded helical bundle. *Nat. Struct. Biol.* **5**, 765 (1998).
7. A. Mayer, W. Wickner, A. Haas, Sec18p (NSF)-driven release of Sec17p (alpha-SNAP) can precede docking and fusion of yeast vacuoles. *Cell* **85**, 83 (1996).
8. I. Dulubova *et al.*, A conformational switch in syntaxin during exocytosis: role of munc18. *EMBO J.* **18**, 4372 (1999).
9. K. M. Misura, R. H. Scheller, W. I. Weis, Three-dimensional structure of the neuronal-Sec1-syntaxin 1a complex. *Nature* **404**, 355 (2000).
10. I. Dulubova *et al.*, Munc18-1 binds directly to the neuronal SNARE complex. *Proc. Natl. Acad. Sci. U. S. A* **104**, 2697 (2007).
11. J. Shen, D. C. Tareste, F. Paumet, J. E. Rothman, T. J. Melia, Selective activation of cognate SNAREpins by Sec1/Munc18 proteins. *Cell* **128**, 183 (2007).
12. J. Basu *et al.*, A minimal domain responsible for Munc13 activity. *Nat. Struct. Mol. Biol.* **12**, 1017 (2005).
13. C. Ma, W. Li, Y. Xu, J. Rizo, Munc13 mediates the transition from the closed syntaxin-Munc18 complex to the SNARE complex. *Nat. Struct. Mol. Biol.* **18**, 542 (2011).
14. R. Fernandez-Chacon *et al.*, Synaptotagmin I functions as a calcium regulator of release probability. *Nature* **410**, 41 (2001).
15. M. Verhage *et al.*, Synaptic assembly of the brain in the absence of neurotransmitter secretion. *Science* **287**, 864 (2000).
16. J. E. Richmond, W. S. Davis, E. M. Jorgensen, UNC-13 is required for synaptic vesicle fusion in C. elegans. *Nat. Neurosci.* **2**, 959 (1999).
17. F. Varoqueaux *et al.*, Total arrest of spontaneous and evoked synaptic transmission but normal synaptogenesis in the absence of Munc13-mediated vesicle priming. *Proc. Natl. Acad. Sci. U. S. A* **99**, 9037 (2002).
18. J. Pei, C. Ma, J. Rizo, N. V. Grishin, Remote homology between Munc13 MUN domain and vesicle tethering complexes. *J. Mol. Biol.* **391**, 509 (2009).

19. W. Li *et al.*, The Crystal Structure of a Munc13 C-terminal Module Exhibits a Remarkable Similarity to Vesicle Tethering Factors. *Structure.* **19**, 1443 (2011).
20. T. Weber *et al.*, SNAREpins: minimal machinery for membrane fusion. *Cell* **92**, 759 (1998).
21. K. L. Boswell *et al.*, Munc13-4 reconstitutes calcium-dependent SNARE-mediated membrane fusion. *J. Cell Biol.* **197**, 301 (2012).
22. M. C. Chicka, E. Hui, H. Liu, E. R. Chapman, Synaptotagmin arrests the SNARE complex before triggering fast, efficient membrane fusion in response to Ca2+. *Nat. Struct. Mol. Biol.* **15**, 827 (2008).
23. A. Stein, A. Radhakrishnan, D. Riedel, D. Fasshauer, R. Jahn, Synaptotagmin activates membrane fusion through a Ca(2+)-dependent trans interaction with phospholipids. *Nat. Struct. Mol. Biol.* **14**, 904 (2007).
24. M. Xue, C. Ma, T. K. Craig, C. Rosenmund, J. Rizo, The Janus-faced nature of the C(2)B domain is fundamental for synaptotagmin-1 function. *Nat. Struct. Mol. Biol.* **15**, 1160 (2008).
25. H. K. Lee *et al.*, Dynamic Ca2+-dependent stimulation of vesicle fusion by membrane-anchored synaptotagmin 1. *Science* **328**, 760 (2010).
26. Diao *et al.*, Synaptic proteins promote calcium-triggered fast transition from point contact to full fusion. e*Life* **1**, e00109 (2012).
27. Materials and methods are available as supplementary materials on *Science* online.
28. T. Weber *et al.*, SNAREpins are functionally resistant to disruption by NSF and alphaSNAP. *J. Cell Biol.* **149**, 1063 (2000).
29. R. Schneggenburger, E. Neher, Presynaptic calcium and control of vesicle fusion. *Curr. Opin. Neurobiol.* **15**, 266 (2005).
30. J. S. Rhee *et al.*, Beta phorbol ester- and diacylglycerol-induced augmentation of transmitter release is mediated by Munc13s and not by PKCs. *Cell* **108**, 121 (2002).
31. O. H. Shin *et al.*, Munc13 C2B domain is an activity-dependent Ca2+ regulator of synaptic exocytosis. *Nat. Struct. Mol. Biol.* **17**, 280 (2010).
32. F. Deak *et al.*, Munc18-1 binding to the neuronal SNARE complex controls synaptic vesicle priming. *J. Cell Biol.* **184**, 751 (2009).
33. T. Ohya *et al.*, Reconstitution of Rab- and SNARE-dependent membrane fusion by synthetic endosomes. *Nature* **459**, 1091 (2009).
34. C. Stroupe, C. M. Hickey, J. Mima, A. S. Burfeind, W. Wickner, Minimal membrane docking requirements revealed by reconstitution of Rab GTPase-dependent membrane fusion from purified components. *Proc. Natl. Acad. Sci. U. S. A* **106**, 17626 (2009).
35. J. Mima, C. M. Hickey, H. Xu, Y. Jun, W. Wickner, Reconstituted membrane fusion requires regulatory lipids, SNAREs and synergistic SNARE chaperones. *EMBO J.* **27**, 2031 (2008).
36. H. Xu, Y. Jun, J. Thompson, J. Yates, W. Wickner, HOPS prevents the disassembly of trans-SNARE complexes by Sec17p/Sec18p during membrane fusion. *EMBO J.* **29**, 1948 (2010).

37. J. Rizo, X. Chen, D. Arac, Unraveling the mechanisms of synaptotagmin and SNARE function in neurotransmitter release. *Trends Cell Biol.* **16**, 339 (2006).

38. X. Chen *et al.*, Three-dimensional structure of the complexin/SNARE complex. *Neuron* **33**, 397 (2002).

39. R. Guan, H. Dai, J. Rizo, Binding of the Munc13-1 MUN Domain to Membrane-Anchored SNARE Complexes. *Biochemistry* **47**, 1474 (2008).

40. X. Chen *et al.*, SNARE-Mediated Lipid Mixing Depends on the Physical State of the Vesicles. *Biophys. J.* **90**, 2062 (2006).

41. Y. Xu, L. Su, J. Rizo, Binding of Munc18-1 to Synaptobrevin and to the SNARE Four-Helix Bundle. *Biochemistry* **49**, 1568 (2010).

42. D. Arac *et al.*, Close membrane-membrane proximity induced by Ca(2+)-dependent multivalent binding of synaptotagmin-1 to phospholipids. *Nat. Struct. Mol. Biol.* **13**, 209 (2006).

43. V. Tugarinov, R. Sprangers, L. E. Kay, Line narrowing in methyl-TROSY using zero-quantum 1H-13C NMR spectroscopy. *J. Am. Chem. Soc.* **126**, 4921 (2004).

44. C. Rickman, B. Davletov, Arachidonic Acid Allows SNARE Complex Formation in the Presence of Munc18. *Chem. Biol.* **12**, 545 (2005).

45. Y. Xu, A. B. Seven, L. Su, Q. X. Jiang, J. Rizo, Membrane bridging and hemifusion by denaturated munc18. *PLoS. ONE.* **6**, e22012 (2011).

46. S. M. Dennison, M. E. Bowen, A. T. Brunger, B. R. Lentz, Neuronal SNAREs Do Not Trigger Fusion between Synthetic Membranes but Do Promote PEG-Mediated Membrane Fusion. *Biophys. J.* **90**, 1661 (2006).

47. J. Diao *et al.*, A single-vesicle content mixing assay for SNARE-mediated membrane fusion. *Nat. Commun.* **1**, 54 (2010).

48. P. C. Zucchi, M. Zick, Membrane fusion catalyzed by a Rab, SNAREs, and SNARE chaperones is accompanied by enhanced permeability to small molecules and by lysis. *Mol. Biol. Cell* **22**, 4635 (2011).

49. F. Parlati *et al.*, Rapid and efficient fusion of phospholipid vesicles by the alpha-helical core of a SNARE complex in the absence of an N-terminal regulatory domain. *Proc. Natl. Acad. Sci. U. S. A* **96**, 12565 (1999).

50. D. Fasshauer, H. Otto, W. K. Eliason, R. Jahn, A. T. Brunger, Structural changes are associated with soluble N-ethylmaleimide-sensitive fusion protein attachment protein receptor complex formation. *J. Biol. Chem.* **272**, 28036 (1997).

51. R. Jahn, R. H. Scheller, SNAREs--engines for membrane fusion. *Nat. Rev. Mol. Cell Biol.* **7**, 631 (2006).

52. K. M. Misura, R. H. Scheller, W. I. Weis, Self-association of the H3 region of syntaxin 1A. Implications for intermediates in SNARE complex assembly. *J. Biol. Chem.* **276**, 13273 (2001).

53. K. M. Misura, L. C. Gonzalez, Jr., A. P. May, R. H. Scheller, W. I. Weis, Crystal structure and biophysical properties of a complex between the N-terminal SNARE region of SNAP25 and syntaxin 1a. *J. Biol. Chem.* **276**, 41301 (2001).

54. F. Zhang, Y. Chen, D. H. Kweon, C. S. Kim, Y. K. Shin, The four-helix bundle of the neuronal target membrane SNARE complex is neither disordered in the middle nor uncoiled at the C-terminal region. *J. Biol. Chem.* **277**, 24294 (2002).

55. A. V. Pobbati, A. Stein, D. Fasshauer, N- to C-terminal SNARE complex assembly promotes rapid membrane fusion. *Science* **313**, 673 (2006).

56. I. Dulubova, T. Yamaguchi, Y. Wang, T. C. Sudhof, J. Rizo, Vam3p structure reveals conserved and divergent properties of syntaxins. *Nat. Struct. Biol.* **8**, 258 (2001).

57. C. M. Carr, E. Grote, M. Munson, F. M. Hughson, P. J. Novick, Sec1p binds to SNARE complexes and concentrates at sites of secretion. *J. Cell Biol.* **146**, 333 (1999).